FATIGUE AND CREEP OF A CONSTRAINED METAL WIRE

A. R. AKISANYA and N. A. FLECK

Cambridge University Engineering Department, Trumpington Street, Cambridge CB2 1PZ, England

(Received 22 June 1992)

Abstract—An experimental investigation has been conducted to examine the enhancement of toughness of composites due to crack bridging under creep and fatigue conditions. The model composite used for the study consists of a metal wire inside a thick-walled glass tube. It is found that the fatigue and the creep resistance of the constrained wire depends upon the failure mechanism. Compared with the unconstrained monolithic wire, the model composite shows greater fatigue and creep strengths due to plastic constraint. The failure stretch of the constrained wire is less for fatigue loading than for monotonic loading; the contribution to toughening is thus reduced under cyclic loading. The failure stretch in creep is dependent only upon the failure mechanism and not upon the applied stress level.

1. INTRODUCTION

The addition of ductile particles or wires to a brittle material can lead to a significant enhancement in toughness of the material. Some engineering materials of practical importance which have been toughened in this way are alumina reinforced with aluminium [1–3], titanium intermetallic alloy reinforced with niobium [4, 5], tungsten carbide reinforced with cobalt [6] and glass reinforced with lead [7].

The enhanced toughness has been attributed to bridging by intact ligaments of the ductile phase in the wake of the crack tip (see Fig. 1). The ductile phase may also increase the toughness by other mechanisms such as crack deflection, crack trapping, plastic straining of particles in the process zone around the crack tip, and by debonding along the particle/matrix interface. The toughness enhancement due to bridging increases with increasing length of the ductile bridging zone behind the crack tip until a steady state toughness is attained at a constant length of bridging zone. The steady state bridging zone size is set by the crack opening displacement, u^*, at which the ductile particles fail. The steady state increase in toughness, ΔG_c, is given in terms of the area fraction f of the ductile ligament intersecting the crack path, the uniaxial yield strength of the unconstrained particle, σ_0, and a representative cross sectional radius of the particle, a_0, by [7]

$$\Delta G_c = f\sigma_0 a_0 W \tag{1}$$

where

$$W = \int_0^{u^*/a_0} \frac{\sigma(u/a_0)}{\sigma_0} \mathrm{d}(u/a_0) \tag{2}$$

is a non-dimensional work of rupture. W varies between 0.5 and 8 depending upon the degree of the constraint experienced during the deformation of the ligament and the constitutive properties of the ductile phase [5, 7]. $\sigma(u/a_0)$ is the nominal stress on the constrained particle at a given normalised crack opening u/a_0. The stress–displacement response of a constrained wire has been shown to differ considerably from that of the unconstrained one [4, 7–9]. The maximum stress, σ_{peak}, on the constrained particle ranges between $1.0\sigma_0$ and $6\sigma_0$ depending upon the extent of the debonding at the particle/matrix interface [5, 7]. The highest value of σ_{peak} is obtained when there is no debonding.

To date, studies on the mechanisms of ductile particle toughening have been devoted to the determination of the non-dimensional work of rupture, W, under a monotonically increasing load [1–7, 10–12]. Large values of W (~ 8) have been obtained for reinforcements that workharden and interfaces that debond readily [5]. Typically, W exhibits a linear dependence upon the debond length, L_d, and upon the normalised plastic stretch to failure of the particle, u^*/a_0.

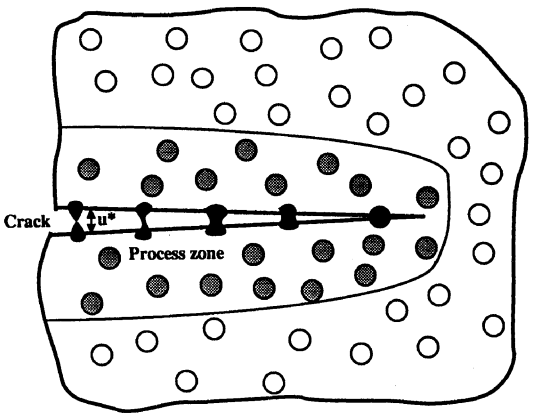

Fig. 1. Crack bridging of brittle matrix by ductile particles.

However, despite the tremendous progress in the understanding of the toughening mechanisms under monotonic loading, there have been few corresponding studies on the fatigue and the creep behaviour of ductile particle reinforced composites. For a titanium intermetallic alloy reinforced with niobium, it has been shown recently [13] that a bridging zone of about 4 mm observed under monotonic loading is diminished to within 150 μm from the crack tip under a cyclic loading. Also, fatigue crack propagation occurs at a stress intensity range below that required for the initiation of crack growth under monotonic loading [13].

In this paper, we investigate the fatigue and the creep behaviour of a constrained lead (Pb) wire. Cylindrical specimens consisting of a lead wire bonded to a thick-walled glass tube [4, 7] are tested under cyclic fatigue loading. In addition, creep rupture tests of the model composite are carried out at room temperature. Monotonic test results for the same model system have previously been reported by Ashby *et al.* [7]. For comparison, further monotonic tests are carried out in this study. To avoid a repetition of the work of Ashby *et al.* [7], only a brief discussion is given of the monotonic test results obtained in the present work. The toughening due to the ductile wire is found to be a strong function of the degree of debonding at the glass/lead interface.

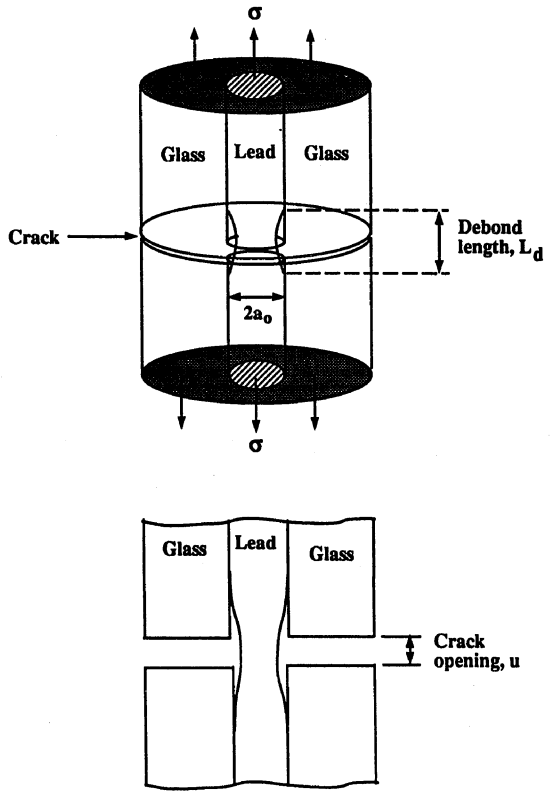

Fig. 2. The test piece. A glass capilliary tube of inner diameter 2.1 mm, and outer diameter 9 mm is filled with lead. σ is the net section stress on the lead wire.

2. EXPERIMENTS

2.1. Specimen geometry and preparation

The geometry of the test specimen is shown in Fig. 2. It consists of a glass circular cylinder reinforced with a central lead wire, and is similar to that used by Ashby *et al.* [7].

Preparation of the specimens was as follows. Glass tubes of length 100 mm, internal diameter 2.1 mm and external diameters 9 mm were cleaned ultrasonically, and then dried in an oven at 300°C for 15 min. The lead (99.999% purity) was melted in an alumina crucible and drawn by suction into the tubes. The tubes were immediately transferred to a furnace at 275°C and cooled slowly to room temperature at 20°C/h. Preliminary tests showed that strong bonding between the glass and the lead required a slow rate of cooling. This is not surprising since there is a large mismatch of coefficients of thermal expansion, α, of the two materials; $\alpha = 5 \times 10^{-6} K^{-1}$ for glass and $\alpha = 29 \times 10^{-6} K^{-1}$ for lead. After cooling, samples were selected in which the lead was free from bubbles, voids or oxide layer over a length of at least 20 mm. A deep notch was scored around the outer circumference of the tube using a glass cutter. The tubes were then adhesively bonded at each end into steel holders. Precracking of the specimen was achieved by a slight bending of the notched glass/lead specimen while in the test grips. The precrack extended from the root of the scored notch up to the reinforcement.

Unconstrained lead wires of 2.1 mm diameter were prepared by coating the inner bore of the glass tube with a "Nicrobraz"† high temperature release agent prior to introduction of the lead. The release agent prevented any bonding between the glass and the lead. The glass/lead specimen was similarly cooled in the oven at a rate of 20°C/h. After manufacture of the glass/lead specimen, a notch was introduced around the circumference of the tube using a glass cutter, and propagated to the glass/lead interface by bending of the glass; the lead was separated from the glass wall by pulling the glass tube at both ends. Finally, the lead wire was cut into specimens of length 25 mm and gauge length 10 mm, and was tested in uniaxial tension, in creep and in fatigue.

2.2. Testing procedures

Monotonic tests of the glass/lead specimens and of the lead wires were performed on a screw-driven machine under displacement control. The tests on the composite cylinder were conducted at a crosshead speed of 8 μms^{-1} while those on the lead wire were conducted at a strain rate of $8 \times 10^{-4} s^{-1}$. For both types of test, the load–displacement curves were recorded.

Cyclic tension–tension and creep tests were performed using a servo hydraulic machine. The cyclic tests were conducted at a constant load range, using

†Made by Wall Colmonoy Limited, Alloy Site, Pontardawe, Glamorgan, Wales.

a constant load ratio R (= minimum load/maximum load) of 0.05 and a frequency of 0.2 Hz (sine wave). The cyclic load–displacement curve was continuously recorded using an X–Y plotter. Creep tests were performed at room temperature, using constant load; the displacement was recorded as a function of time on a chart recorder.

The fracture surfaces of the specimens were examined in a scanning electron microscope (SEM). The extent of the debonding along the glass/lead interface was determined by injecting an alcohol-based ink on the fracture surface. The ink penetrated into the debonded region, and the debend length was then measured using a travelling microscope to an accuracy of 0.01 mm.

3. RESULTS AND DISCUSSION

3.1. Monotonic tests

3.1.1. Unconstrained wire. Tensile tests on the unconstrained lead gave the nominal stress–strain curves shown in Fig. 3. The specimens failed by necking down to a point. The uniaxial yield stress of the unconstrained lead σ_0 equals 4.6 ± 0.5 MPa and the ultimate tensile strength (UTS) of the lead is 13 ± 4 MPa. For straining beyond yield and before the point of necking, the true stress σ_t vs total true strain ϵ_t is given by $\sigma_t = A\epsilon_t^n$ where $A = 15 \pm 4$ MPa and $n = 0.21$. Thus, the wire exhibits appreciable strain hardening.

3.1.2. Composite cylinders (constrained wire). The composite cylinders failed by three distinct mechanisms, as previously observed by Ashby *et al.* [7]. Typical fracture surfaces are shown in Fig. 4. When the adhesion between the glass and the lead was good, a large single void was nucleated within the lead, Fig. 4(a). Occasionally, the lead remained bonded to the glass and the growth of the internal void was accompanied by the formation of concentric cracks in the glass, Fig. 4(b). Debonding between the glass and

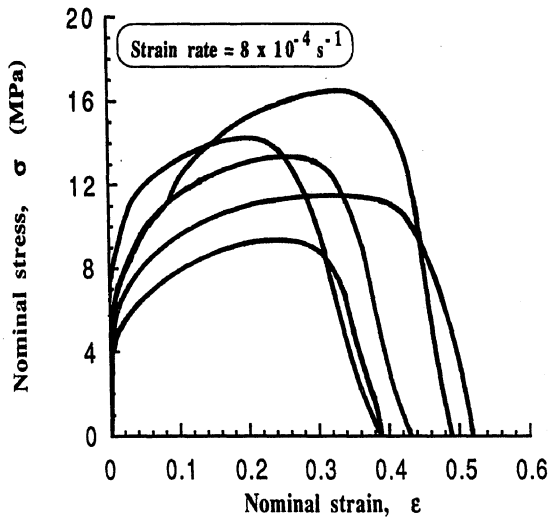

Fig. 3. Nominal stress–strain curves for the unconstrained lead wire. The gauge length is 10 mm.

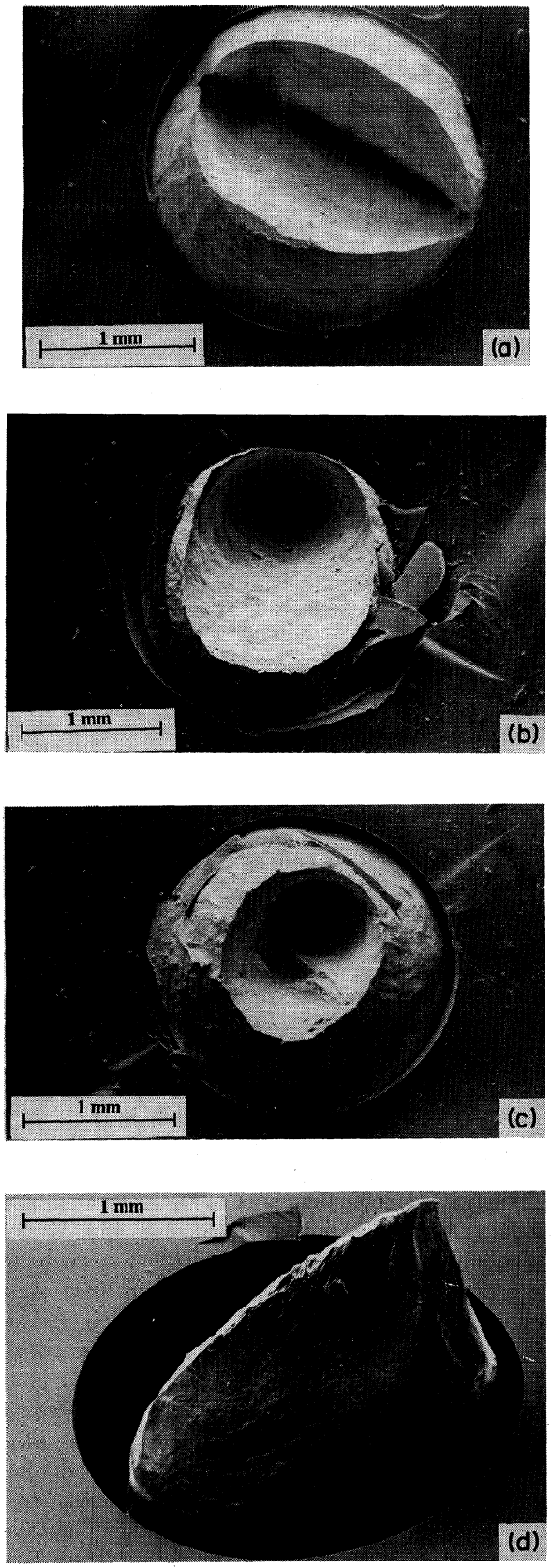

Fig. 4. Fracture surfaces of the constrained lead wire under monotonic loading. (a) Failure by the growth of a single internal void with no debonding at the glass/lead interface. (b) Failure by the growth of internal void accompanied by the formation of concentric cracks in the glass. There is no debonding at the interface. (c) Limited debonding at the interface accompanied by the growth of a single internal void. (d) Extensive debonding at the interface coupled with the necking of the lead wire.

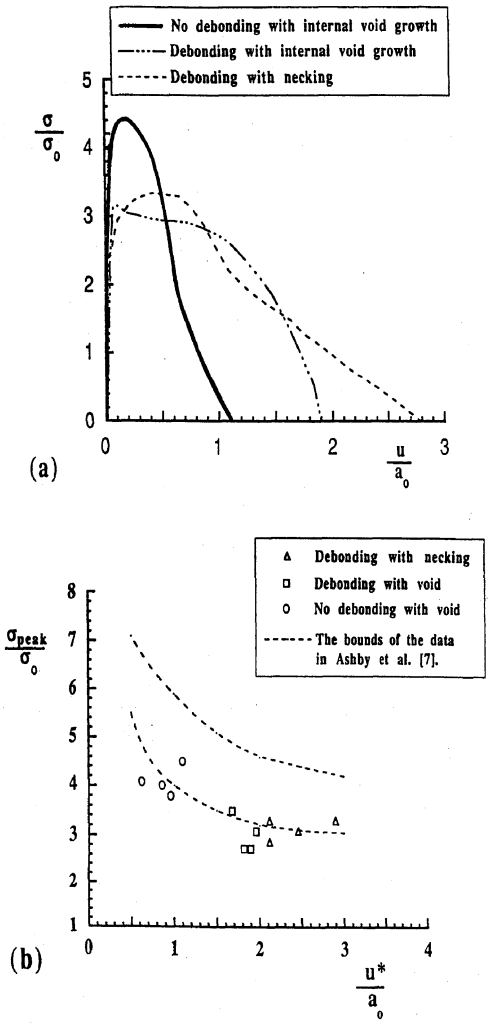

Fig. 5. (a) Typical normalised stress–displacement curves for the glass/lead composite cylinders. $\sigma_0 (= 4.6\,\text{MPa})$ and $a_0 (= 1.1\,\text{mm})$ are the uniaxial yield strength and the radius of the unconstrained wire, respectively. (b) The normalised peak stress, σ_{peak}/σ_0, against the normalised opening displacement at failure, u^*/a_0.

the lead occurred when the glass/lead interface was weak. Limited debonding was always accompanied by the growth of an internal void, Fig. 4(c). When debonding was extensive, the lead drew down to a knife-edge or a point, and no central void was formed, as shown in Fig. 4(d).

Typical stress–displacement curves for the composite cylinder are shown in Fig. 5(a). Here, we plot the nominal stress σ based on the initial cross-sectional area of the lead in the capillary tube against the relative displacement u of the two ends of the specimen. The relative displacement u closely approximates the "crack opening displacement" across the crack in the glass tube. The nominal stress σ has been normalised by the uniaxial yield strength of the unconstrained lead, $\sigma_0 = 4.6\,\text{MPa}$, while the crack opening displacement u has been normalised by the initial radius of the wire, $a_0 = 1.1\,\text{mm}$. The shape of the curves are dependent upon the three failure mechanisms described above: good adhesion between the glass and the lead but with the growth of an internal void [see Fig. 4(a)], limited debonding with an internal void [Fig. 4(c)], and extensive debonding with necking [Fig. 4(d)]. In all cases the normalised stress σ/σ_0 initially rises to a peak value at a normalized displacement u/a_0 ranging from 0.05 to 0.3, and then falls until the wire fails at a maximum opening displacement u^*/a_0. The peak stress σ_{peak}/σ_0 is between 4 and 5 when there is no debonding, 2.5 and 3.5 when there is minimal debonding, and 3 and 3.5 when debonding is extensive.

The normalised peak stress, σ_{peak}/σ_0, is plotted against the normalised opening displacement at failure, u^*/a_0, in Fig. 5(b). The peak stress, σ_{peak}/σ_0, decreases while the failure stretch, u^*/a_0, increases as the constraint between the glass and the lead is lost due to debonding at the glass/lead interface. The trends in σ_{peak}/σ_0 vs u^*/a_0 reported by Ashby *et al.* [7] are included in Fig. 5(b). The lower values of σ_{peak}/σ_0 obtained in the present study compared to those by Ashby *et al.* [7] are attributed, probably, to the different technique of precracking. The bending of the specimen may result in some loss of constraint between the glass and the lead.

The steady state toughness increase due to bridging depends upon the work of rupture parameter, W as demonstrated by equations (1) and (2). Extensive debonding at the glass/lead interface increases the gauge length over which plastic deformation of the wire occurs, and hence increases both the stretch to failure of the wire and the work of rupture. We find that both the stretch to failure u^*/a_0 and the work of rupture parameter W increase linearly with the debond length L_d/a_0 (see Fig. 6). The empirical fits

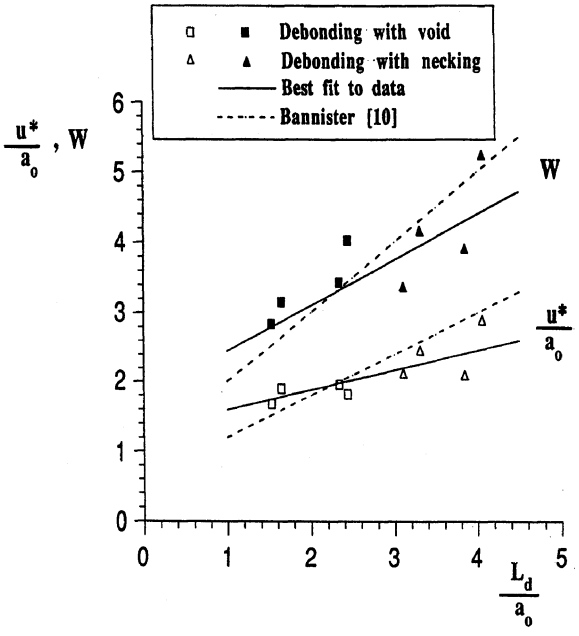

Fig. 6. The effect of the normalised debond length L_d/a_0 upon the normalised displacement at failure, u^*/a_0, and upon the work of rupture parameter, W, under monotonic loading. The solid symbols correspond to W while the open symbols are for u^*/a_0.

to the data of Fig. 6 are given by

$$\frac{u^*}{a_0} = 1.3 + 0.29\frac{L_d}{a_0} \tag{3}$$

and

$$W = 1.8 + 0.65\frac{L_d}{a_0}. \tag{4}$$

A similar linear dependence of u^*/a_0 and of W upon the debond length L_d/a_0 has been observed by Bannister [10] in tests of lead sheet sandwiched between two glass plates. The trends in u^*/a_0 and W vs L_d/a_0 reported by Bannister [10] are included in Fig. 6. The correlation between the present results and those of [10] demonstrates that the linear dependence of u^*/a_0 and W upon the debond length is independent of the specimen geometry.

The results plotted in Fig. 6 show that the increase in toughness due to bridging, ΔG_c, can be maximized by allowing some debonding between the matrix and the wire or particle. However, debonding results in a composite of low tensile strength. Therefore a compromise has to be reached between arranging for full constraint between the particle and the matrix giving *low toughness* and *high strength*, and partial debonding which gives *high toughness* and *low strength*. A dual reinforcement scheme has recently been suggested [5] where one reinforcement debonds and contributes to the toughness and the other bonds well and contributes to the strength. The toughening characteristics of such a dual-reinforced material are yet to be addressed.

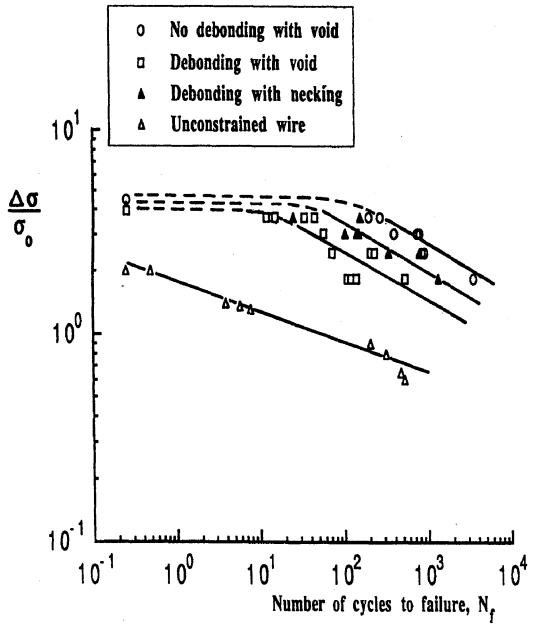

Fig. 7. The S–N curves for both the constrained and the unconstrained lead wires. The solid lines are the best fit to the experimental data, while the dashed lines are the extrapolation of the experimental data to the peak stress under monotonic loading at a quarter of a cycle. The stress ratio R ($=\sigma_{min}/\sigma_{max}$) is 0.05 and the tests were conducted at a frequency of 0.2 Hz (sine wave).

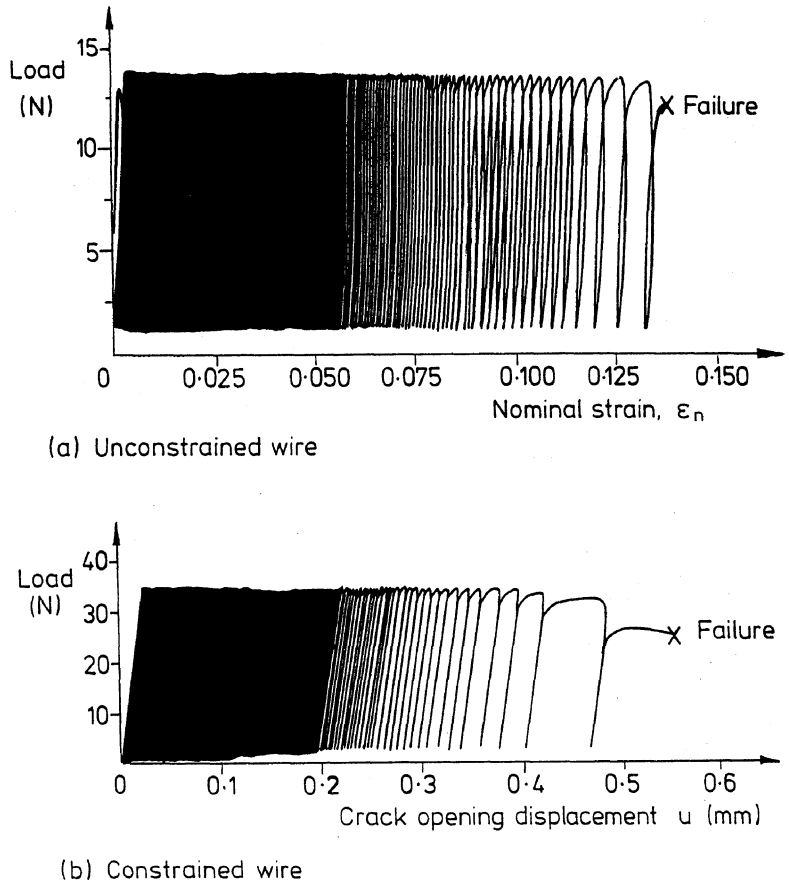

Fig. 8. Typical cyclic load–displacement curves for the constrained and the unconstrained lead wires.

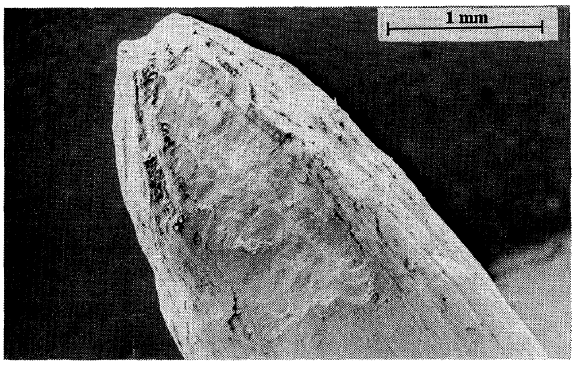

Fig. 9. Fracture surface of the unconstrained lead wire under cyclic loading.

3.2. Fatigue behaviour

3.2.1. Unconstrained wire. The cyclic stress-life (S–N) curve for the unconstrained lead is shown in Fig. 7. The number of cycles to failure N_f decreases as the nominal stress range $\Delta\sigma$ $(=\sigma_{max}-\sigma_{min})$ increases. The specimens accumulated plastic strain by ratchetting, until failure occurred by necking to a point. A typical cyclic load–displacement curve is shown in Fig. 8(a) while the fracture surface of a necked specimen is shown in Fig. 9. Microscopic examination of the fracture surface showed no evidence of slip steps or striations. The nominal strain at failure, $\epsilon^* = u^*/l_0$, is between 0.3 and 0.7, and is independent of the stress range $\Delta\sigma$ applied to the specimen. Here, u^* is the extension at failure and l_0 ($= 10$ mm) is the initial gauge length of the specimen. These values for ϵ^* under cyclic loading are within the range obtained under monotonic loading; for the monotonic tests, $\epsilon^* = 0.39 - 0.52$ as shown in Fig. 3.

3.2.2. Composite cylinders (constrained wire). The S–N curves for the glass/lead specimens are included in Fig. 7. The specimens failed by three mechanisms similar to those observed under monotonic loading. The mechanisms are: (a) no debonding with internal void growth, (b) minimal debonding with internal

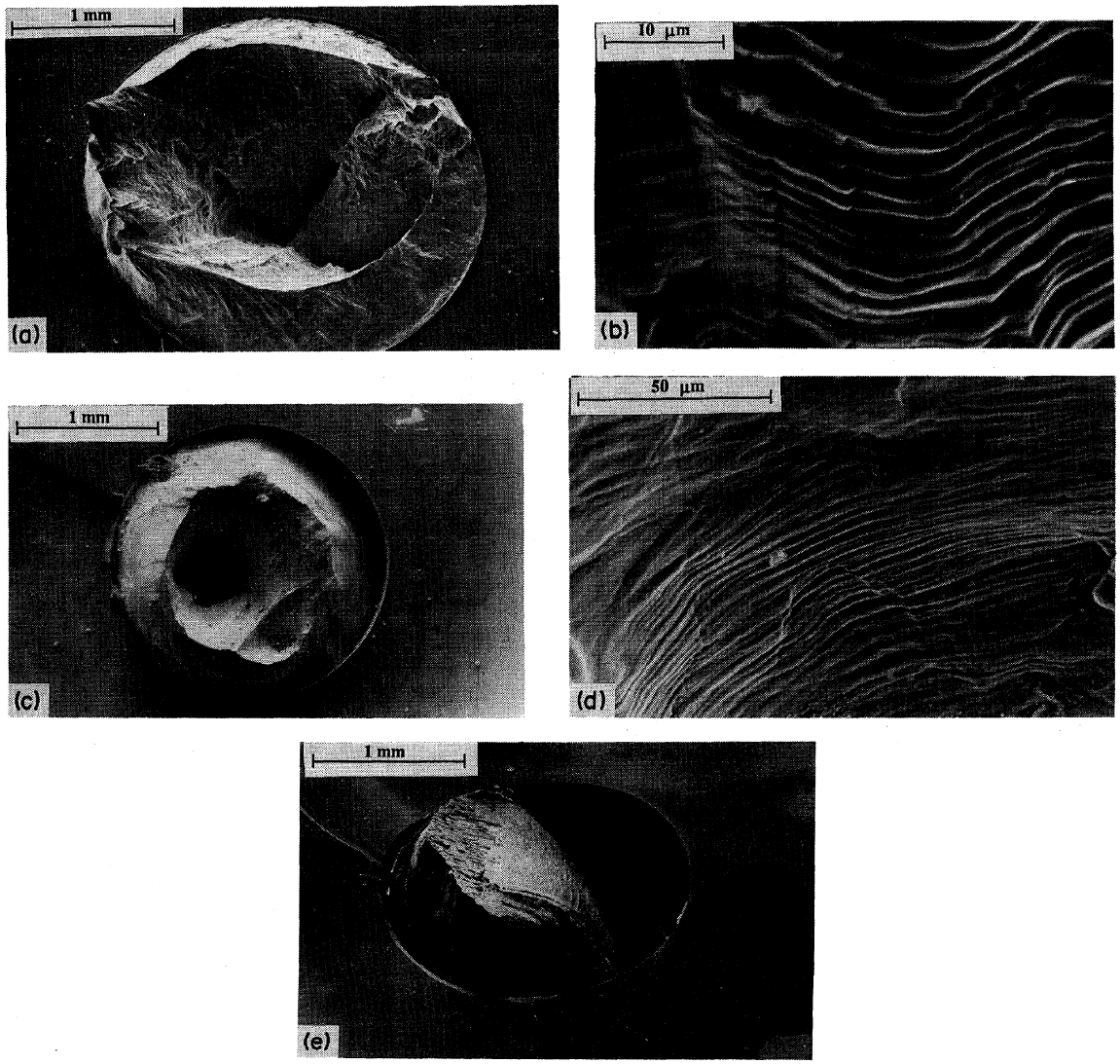

Fig. 10. Fracture surfaces of the constrained lead wire in fatigue. (a) Failure by the growth of a single void with no debonding at the interface. (b) Magnified view of the circled part of (a). Fatigue striations show the growth of the void with increasing number of fatigue cycles. (c) Minimal debonding at the interface with void growth in the lead. (d) Magnified view of the circled part of (c) showing fatigue striations. (e) Extensive debonding at the interface with necking of the lead.

void growth, and (c) extensive debonding with necking. Micrographs of the failure surfaces are shown in Fig. 10. The fatigue strength of the constrained wires was greater than that of the unconstrained wires. The greatest resistance to fatigue was obtained when the adhesion between the glass and the lead was good and the specimen failed by the progressive growth of an internal void, Fig. 10(a). The resistance to fatigue was lowest for the case of partial debonding accompanied with void growth. In this case, minimal debonding results in a partial loss of constraint between the glass and the lead, and hence a reduction in the maximum stress that the specimen can withstand (see Fig. 5). In addition, the growth of the void results in the concentration of cyclic plastic strain around the remaining small cylindrical ligament of the wire.

The growth of the void with increasing number of fatigue cycles is evident from the striations shown in Fig. 10(b, d). The spacing of the striations ranges between 1 and 3 μm. Microscopic examination at high magnification of the glass/lead specimens that failed by debonding and necking also revealed the presence of striations on the fracture surface (not shown in Fig. 10).

The S–N curves can be fitted to an equation of the form

$$\left(\frac{\Delta\sigma}{\sigma_0}\right) N_f^{\beta} = C \qquad (5)$$

where σ_0 is the uniaxial yield stress of the unconstrained wire. C and β are empirical constants which depend upon the failure mechanism. We deduce from Fig. 7 that for the constrained wire (C, β) takes the values (16, 0.5), (9, 0.5) and (6.5, 0.5) for (a) no debonding with internal void growth, (b) minimal debonding with void growth, and (c) extensive debonding with necking, respectively. The S–N curve for the unconstrained wire is described by equation (5) with $\beta = 0.36$ and $C = 1.8$ cycle$^{\beta}$.

The cyclic load–displacement curves [see Fig. 8(b)] showed that the composite specimens failed by the cyclic accumulation of plastic strain in the direction of the applied load as in the case of the unconstrained wire. The maximum displacement, in each fatigue cycle u_{max} increases with increasing number of fatigue cycles until failure occurs, as shown in Fig. 11(a). When the specimen fails by debonding and necking, a transient region occurs in which the ratchetting rate, $d(u_{max}/a_0)/dN$, diminishes with increasing opening displacement at fixed stress amplitude, followed by a steady state region in which $d(u_{max}/a_0)/dN$ remains constant. In contrast, specimens that fail by debonding and void growth exhibit a negligible transient; the ratchetting rate remains constant with increasing number of fatigue cycles except when the maximum displacement u_{max} approaches the failure displacement u^*. The steady state rate of ratchetting $d(u_{max}/a_0)/dN$ is plotted as a function of the normalised stress range $\Delta\sigma/\sigma_0$ in Fig. 11(b). The ratchetting rate for the specimens that fail by debonding and

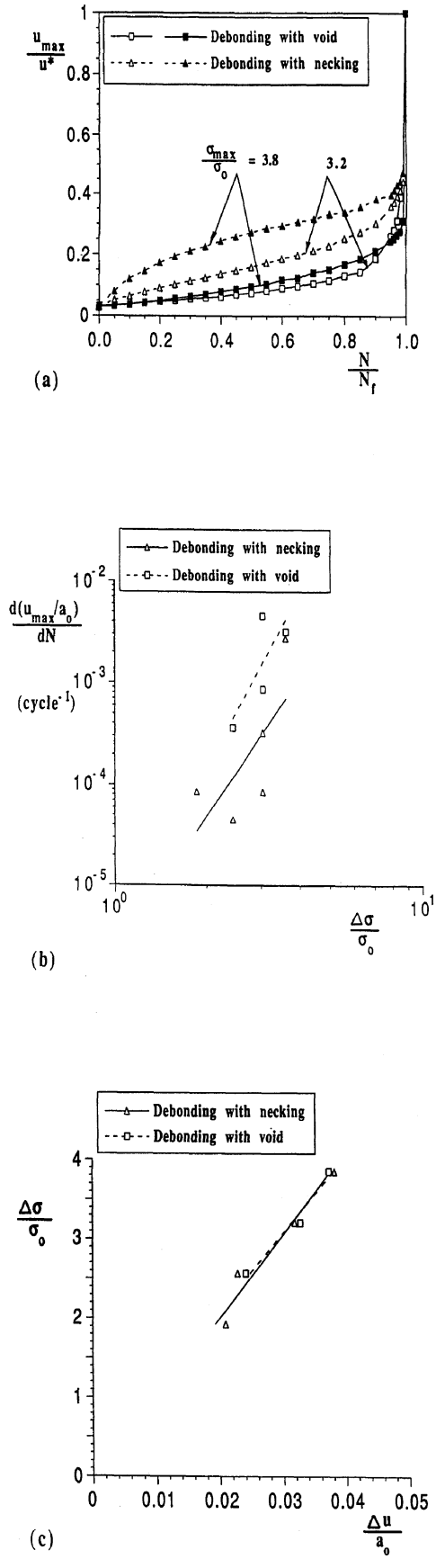

Fig. 11. (a) A plot of the normalised maximum opening displacement in each fatigue cycle vs the normalised number of fatigue cycles for the constrained wire. (b) Effect of the normalised stress range upon the steady state rate of ratchetting. (c) A plot of the normalised cyclic stress–displacement range.

internal void growth is higher than the rate for the specimens that fail by debonding and necking. The ratchetting rate vs the stress range curves can be fitted to a power law equation of the form

$$\frac{d(u_{max}/a_0)}{dN} = B\left(\frac{\Delta\sigma}{\sigma_0}\right)^s \tag{6}$$

where B and s are empirical constants which are dependent upon the failure mechanism. The data plotted in Fig. 11(b) suggest (B, s) values of $(3 \times 10^{-6}, 5.6)$ and $(2 \times 10^{-6}, 4.5)$ for the case of debonding with void growth, and extensive debonding with necking, respectively. We note that the displacement range Δu $(= u_{max} - u_{min})$ remains constant with increasing number of fatigue cycles, and is linearly dependent upon the stress range $\Delta\sigma$, as shown in Fig. 11(c). The displacement range is not dependent upon the failure mechanism. The results can be summarised by the equation

$$\frac{\Delta\sigma}{\sigma_0} = 100\frac{\Delta u}{a_0}. \tag{7}$$

Current theories of crack briding under fatigue conditions [14] assume a cyclic traction–displacement law for the bridging particles and neglect the phenomenon of ratchetting. This is reasonable if the mean stress relaxes quickly by ratchetting and the bridged material suffers fully reversed low cycle fatigue. If, however, ratchetting is slow then a more complex description of the bridging law is required in order to include the effect of ratchetting. A suitable measure of the significance of ratchetting is the ratio of the displacement range Δu per load cycle and the accumulated displacement δu_{max} per load cycle. For the constrained lead wire, $\Delta u \ll \delta u_{max}$. This implies that for the case of wire reinforced composite, ratchetting of the constrained wires occurs rapidly behind the crack tip; the mean stress of the wires quickly relaxes to zero and the wires fail by low cycle fatigue.

Under monotonic loading, a peak stress of the order of $\sigma_{peak}/\sigma_0 \sim 4.5$ is attained before failure. However, the susceptibility of the constrained wire to fatigue implies that the wire fails at a lower load if subjected to a sufficient number of fatigue cycles (see Fig. 7). We deduce that fatigue crack growth may occur in a ductile particle toughened composite at a lower range of stress intensity factor than under monotonic loading; the contribution to toughening due to bridging is reduced under fatigue loading.

The crack opening displacement at which the wire fails, u^*/a_0, is plotted in Fig. 12(a) for different values of the normalised stress range $\Delta\sigma/\sigma_0$. For all three failure mechanisms, u^*/a_0 increases as $\Delta\sigma/\sigma_0$ increases. As in the static case, u^*/a_0 has the largest value when the specimen debonded and necked, and the lowest value when there was no debonding with internal void growth. The low values of u^*/a_0 at low load ranges imply that the bridging zone size in fatigue is smaller than the bridging zone size for

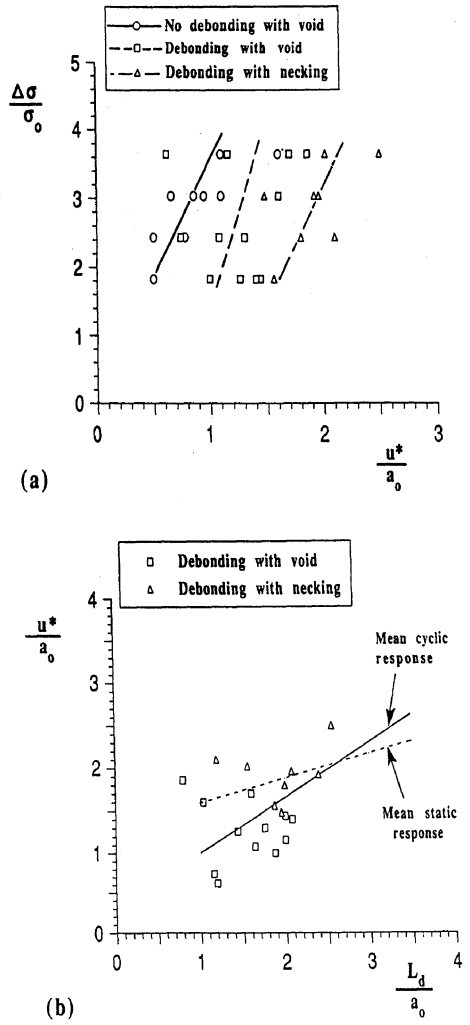

Fig. 12. The dependence of the normalised opening displacement at failure, u^*/a_0, under cyclic loading upon (a) the normalised stress range $\Delta\sigma/\sigma_0$, and (b) the normalised debond length L_d/a_0. The solid and the dashed lines in (a) are best fits to the experimental data.

monotonic loading. This is consistent with the experimental observation of the fatigue behaviour of a TiAl intermetallic alloy reinforced with TiNb particles [13]. A bridging zone of about 4 mm under monotonic loading diminished under fatigue loading to 150 μm behind the crack tip.

The crack opening displacement at failure under cyclic loading shows a linear dependence upon the debond length, L_d/a_0, as in the monotonic loading, Fig. 12(b). The best fit to the fatigue data is given by

$$\frac{u^*}{a_0} = 0.3 + 0.65\frac{L_d}{a_0}. \tag{8}$$

The final debond length is expected to depend upon the distribution of flaws along the glass/lead interface. Adequate characterisation of the interface is thus necessary. The debond lengths L_d/a_0 plotted in Fig. 12(b) are the values at failure. It is not clear whether debonding increases with increasing number of fatigue cycles. Further experiments using a different specimen geometry are needed to quantify interfacial fatigue crack growth.

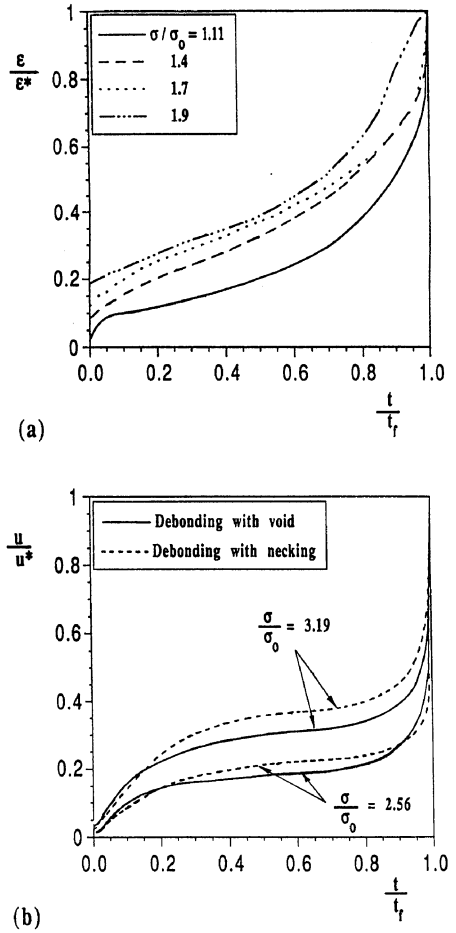

Fig. 13. (a) The normalized nominal strain against the normalised time for the unconstrained lead wire. The gauge length is 10 mm. ϵ^* and t_f are the nominal strain at, and the time to failure, respectively. (b) The normalised opening displacement against the normalised time for the constrained wire. The tests in (a) and (b) were conducted at room temperature; $T \approx 25°C$.

3.3. Creep behaviour

3.3.1. Constrained wire. The creep response of the unconstrained wire is shown in Fig. 13(a) for constant applied load. The strain, ϵ, is normalised by the failure strain, ϵ^*, while the time, t, is normalised by the time to failure, t_f. The strain increases with time until failure occurs by necking. The strain rate decreases with time in the initial primary creep regime, and later settles down to a constant value (secondary creep) before increasing rapidly as the failure strain is approached. The steady state strain rate $\dot{\epsilon}_{ss}$ is related to the normalised applied stress σ/σ_0 by

$$\frac{\dot{\epsilon}_{ss}}{\dot{\epsilon}_{ref}} = 8.2 \times 10^{-6}\left(\frac{\sigma}{\sigma_0}\right)^{7.1} \tag{9}$$

where the reference strain rate is $\dot{\epsilon}_{ref} = 1\ s^{-1}$.

The normalised applied stress σ/σ_0 is plotted against the time to failure t_f in Fig. 14(a). The time to failure decreases with increasing stress on the specimen. The best fit to the data shows that the time to failure t_f (s) is related to the normalised applied stress σ/σ_0 by

$$t_f = 1.7 \times 10^4\left(\frac{\sigma}{\sigma_0}\right)^{-6.9}. \tag{10}$$

3.3.2. Composite cylinders (constrained wire). The glass/lead specimens failed in creep by two mechanisms: (a) minimal debonding with void growth [see Fig. 15(a)], and (b) extensive debonding with necking [see Fig. 15(b)]. The normalised applied stress σ/σ_0 vs the time to failure t_f curves for the constrained wire are included in Fig. 14(a). The constrained wire shows creep strengths which are typically three times that of the unconstrained wire. The failure time t_f (s) for the constrained wire is related to the normalised applied stress by

$$t_f = 2.1 \times 10^5\left(\frac{\sigma}{\sigma_0}\right)^{-4.6} \tag{11}$$

for the case of minimal debonding with internal void growth, and by

$$t_f = 1.8 \times 10^5\left(\frac{\sigma}{\sigma_0}\right)^{-3.1} \tag{12}$$

for the case of extensive debonding with necking.

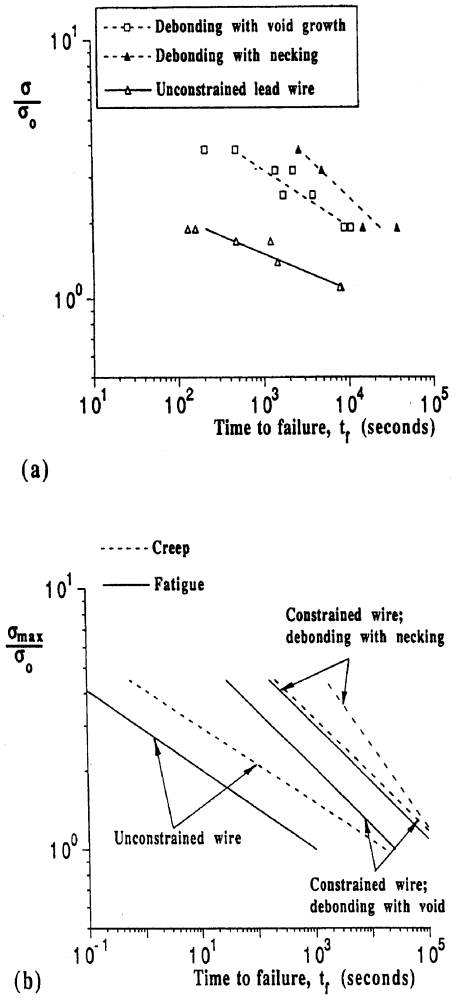

Fig. 14. (a) Effect of the normalised applied stress σ/σ_0 upon the time to failure t_f for the unconstrained wire and the model composite specimens. The solid lines are best fits to the experimental data. (b) Comparison between the time to failure in fatigue and in creep.

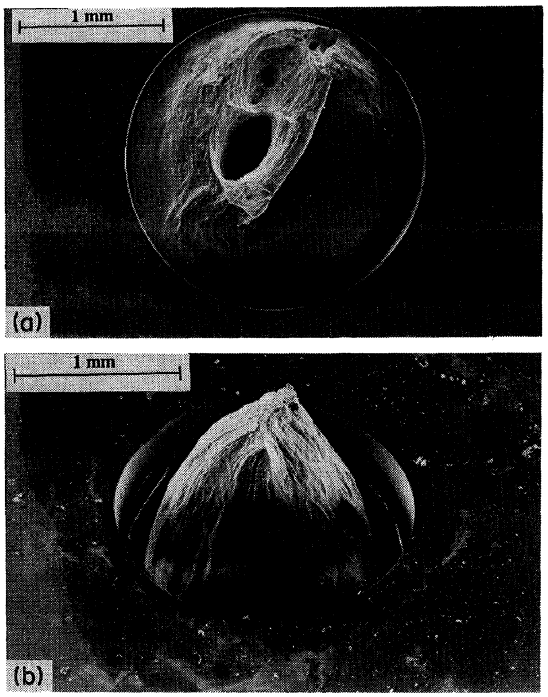

Fig. 15. Fracture surfaces of the constrained wire in creep. (a) Debonding with internal void growth, and (b) debonding with necking.

Figure 14(b) shows the comparison between the time to failure in fatigue and in creep for the monolithic lead wire and the constrained wire. There is minimal fatigue-creep interaction by the following argument. If we assume that ratchetting is by creep and not by fatigue, a linear summation of damage would give fatigue lives about 100 times longer than those actually observed.

Typical crack opening displacement u vs time curves are shown in Fig. 13(b) for the constrained wires. As for the unconstrained wires, primary, secondary and tertiary creep regimes are evident. The normalised steady state opening displacement rate $\dot{u}/a_0$ (in secondary creep) is plotted against the normalised applied stress σ/σ_0 in Fig. 16(a). Specimens that fail by minimal debonding with internal void growth display greater displacement rates (and shorter creep lives) than those that fail by debonding and necking. The steady state crack opening displacement rate of the constrained wire in creep, $\dot{u}/a_0$, is related to the normalised applied stress by

$$\frac{\dot{u}}{\dot{\epsilon}_{\text{ref}} a_0} = 0.91 \times 10^{-6} \left(\frac{\sigma}{\sigma_0}\right)^{4.95} \tag{13}$$

for the case of debonding with void growth, and by

$$\frac{\dot{u}}{\dot{\epsilon}_{\text{ref}} a_0} = 1.3 \times 10^{-6} \left(\frac{\sigma}{\sigma_0}\right)^{2.92} \tag{14}$$

for the case of debonding with necking. The reference strain rate $\dot{\epsilon}_{\text{ref}} = 1\text{s}^{-1}$.

Figure 16(b) shows the failure stretch from the monotonic, fatigue and creep tests. The failure stretch u^*/a_0 in creep remains fairly constant for all values of the applied stress, and is equal to the monotonic

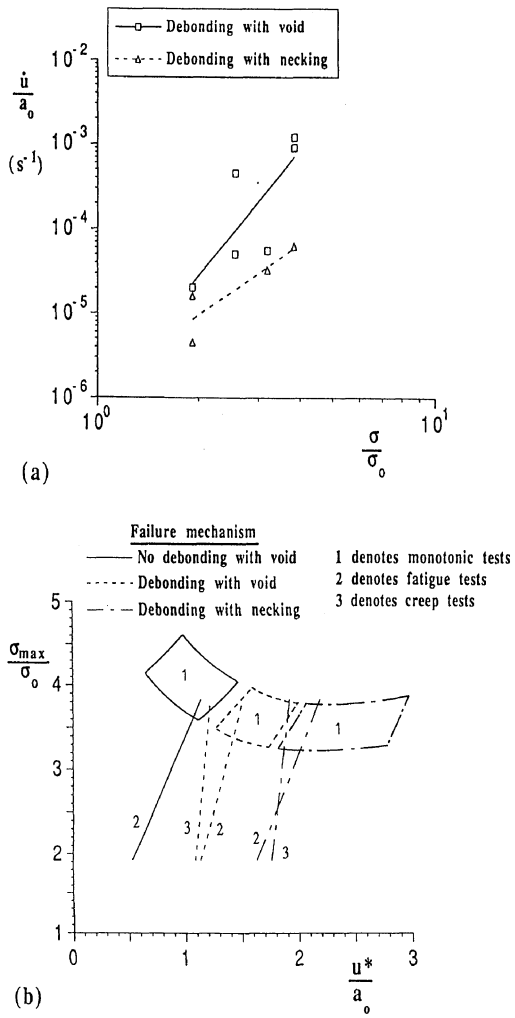

Fig. 16. Effect of the normalised applied stress σ/σ_0 upon (a) the steady state crack opening displacement rate $\dot{u}/a_0$ for the constrained wire in creep, and (b) upon the failure stretch of the constrained wire under monotonic loading (lines no. 1), fatigue loading (lines no. 2), and creep loading (lines no. 3).

failure stretch to within experimental scatter. We note that for monotonic, fatigue and creep tests, the specimens that fail by debonding and necking possess the highest failure displacements. We further deduce from Fig. 16(b) that the bridging enhancement to toughness of a fibre composite is greatest for monotonic loading, and is significantly reduced for fatigue or creep loading.

4. CONCLUDING REMARKS

The present experiments clarify the fatigue and creep characteristics of a ductile particle reinforced material. The response bears many similarities to the behaviour under monotonic loading. Under monotonic loading, the peak stress carried by the constrained lead wire is approximately 4 times the yield stress of the unconstrained lead. The model composite maintains this high plastic constraint under fatigue and creep loading.

Three failure mechanisms are observed under monotonic and fatigue loading: no debonding with internal void growth, minimal debonding with internal void growth and extensive debonding with necking. Under creep loading, failure is by minimal debonding with internal void growth and extensive debonding with necking.

Under fatigue and creep loading the work of rupture W is reduced; hence the enhancement of toughness of a fibre (or particle) reinforced composite due to bridging is reduced. Toughened composites typically experience fatigue and creep loading in service; alternative means must be sought to increase the toughness of composites under these circumstances.

Acknowledgements—The authors are grateful for several helpful discussions with Professors J. W. Hutchinson and M. F. Ashby, and also with Drs B. N. Cox and H. R. Shercliff. ARA acknowledges the financial support of the Cambridge Commonwealth Trust.

REFERENCES

1. M. S. Newkirk, A. W. Urqhart and H. R. Zwicker, *J. Mater. Res.* **1,** 81 (1986).
2. L. S. Sigl, P. A. Mataga, B. J. Dalgleish, R. M. McMeeking and A. G. Evans, *Acta metall.* **36,** 945 (1988).
3. B. D. Flinn, M. Rühle and A. G. Evans, *Acta metall.* **37,** 3001 (1989).
4. H. C. Cao, B. J. Dalgleish, H. E. Deve, C. Elliott, A. G. Evans, R. Mehrabian and G. R. Odette, *Acta metall.* **37,** 2696 (1989).
5. H. E. Deve, A. G. Evans, G. R. Odette, R. Mehrabian, M. L. Emiliani and R. J. Hecht, *Acta metall.* **38,** 1491 (1990).
6. L. S. Sigl and H. E. Exner, *Metall. Trans.* **18A,** 1299 (1987).
7. M. F. Ashby, F. J. Blunt and M. Bannister, *Acta metall.* **37,** 1847 (1989).
8. A. G. Evans and R. M. McMeeking, *Acta metall.* **34,** 2435 (1988).
9. P. W. Bridgeman, *Studies of Large Plastic Flow and Fracture.* Harvard Univ. Press (1964).
10. M. K. Bannister, Ph.D. thesis, Cambridge Univ. (1990).
11. F. Zok and C. L. Hom, *Acta metall.* **38,** 1895 (1990).
12. B. Budiansky, J. C. Amazigo and A. G. Evans, *J. Mech. Phys. Solids* **36,** 167 (1988).
13. K. T. V. Rao, G. R. Odette and R. O. Ritchie, *Acta metall. mater.* **40,** 353 (1992).
14. R. M. McMeeking and A. G. Evans, *Mech. Mater.* **9,** 217 (1990).